Advances in Water Resources 57 (2013) 41–51

Contents lists available at SciVerse ScienceDirect

Advances in Water Resources

journal homepage: www.elsevier.com/locate/advwatres

Generalized martingale model of the uncertainty evolution of streamflow forecasts

Tongtiegang Zhao [a], Jianshi Zhao [a,*], Dawen Yang [a], Hao Wang [a,b]

[a] State key Laboratory of Hydro-Science and Engineering, Department of Hydraulic Engineering, Tsinghua University, Beijing, China
[b] State Key Laboratory of Simulation and Regulation of Water Cycle in River Basin, China Institute of Water Resources and Hydropower Research, Beijing, China

ARTICLE INFO

Article history:
Received 14 July 2012
Received in revised form 15 January 2013
Accepted 24 March 2013
Available online 31 March 2013

Keywords:
Forecast uncertainty
Forecast improvement
Martingale model of forecast evolution
Normal quantile transform
Rolling horizon reservoir operation

ABSTRACT

Streamflow forecasts are dynamically updated in real-time, thus facilitating a process of forecast uncertainty evolution. Forecast uncertainty generally decreases over time and as more hydrologic information becomes available. The process of forecasting and uncertainty updating can be described by the martingale model of forecast evolution (MMFE), which formulates the total forecast uncertainty of a streamflow in one future period as the sum of forecast improvements in the intermediate periods. This study tests the assumptions, i.e., unbiasedness, Gaussianity, temporal independence, and stationarity, of MMFE using real-world streamflow forecast data. The results show that (1) real-world forecasts can be biased and tend to underestimate the actual streamflow, and (2) real-world forecast uncertainty is non-Gaussian and heavy-tailed. Based on these statistical tests, this study proposes a generalized martingale model GMMFE for the simulation of biased and non-Gaussian forecast uncertainties. The new model combines the normal quantile transform (NQT) with MMFE to formulate the uncertainty evolution of real-world streamflow forecasts. Reservoir operations based on a synthetic forecast by GMMFE illustrates that applications of streamflow forecasting facilitate utility improvements and that special attention should be focused on the statistical distribution of forecast uncertainty.

1. Introduction

Streamflow forecasts provide useful information about the future. Forecasts are especially important for predicting extreme hydrologic events and are used to guide management decisions on water resource systems [3,4,14]. Advances in weather forecasting, hydrologic modeling, and hydro-climatic teleconnections have improved the ability to forecast streamflows [6,23,25]. As a result, streamflow forecasts have been extensively applied in water resource management. The applications usually take a two-component approach. One paper develops innovative models for streamflow forecasting, whereas the other proposes novel optimization models to incorporate the forecast into decision making. For example, Carpenter and Georgakakos [6] generated an ensemble streamflow forecast that considered both atmospheric forcing and hydrologic model uncertainty. Yao and Georgakakos [26] then developed forecast-management schemes with operation rules and optimization models. Maurer and Lettenmaier [13] assessed the seasonal streamflow predictability of the Mississippi River basin. Based on these data, [14] evaluated the value of seasonal streamflow forecast to guide the Missouri River main-stem reservoir operation. Ajami et al. [1] proposed an integrated Bayesian uncertainty estimator to account for input, parameter, and model structural uncertainty in hydrologic prediction, after which they demonstrated the importance of considering hydrological uncertainty in sustainable water resource management [2].

Uncertainty is an inherent and important characteristic of streamflow forecasting. In both real-world and hypothetical studies focusing on the applications of streamflow forecasting, uncertainty has been identified as the major influencing factor of the value of the forecast [2,16,27]. Real-world studies that aim to develop decision support systems for a targeted river basin generally address forecast uncertainty using advanced forecast techniques (e.g., ensemble forecasts) and optimization (or simulation) models [3,20,26]. Hypothetical studies typically use synthesized forecast uncertainty based on certain assumptions, e.g., unbiasedness, and Gaussian distributions [12,24,27]. Testing the validity of these assumptions is an important issue for this type of hypothetical study. In this investigation, we use real-world forecast data and perform statistical tests on assumptions of forecast uncertainty.

Forecast uncertainty evolves in real-time because streamflow forecasts are dynamically updated. On one hand, the uncertainties of forecasts for future periods become larger as forecast lead-time increases. On the other hand, the uncertainties of forecasts for a certain time period decrease over time as more hydrologic information becomes available. Heath and Jackson [8] proposed a

* Corresponding author. Tel.: +86 10 62796539; fax: +86 10 62796971.
E-mail address: zhaojianshi@tsinghua.edu.cn (J. Zhao).

0309-1708/$ - see front matter © 2013 Elsevier Ltd. All rights reserved.
http://dx.doi.org/10.1016/j.advwatres.2013.03.008

martingale model of forecast evolution (MMFE) to formulate the uncertainty evolution of demand forecasts in supply chain management. Zhao et al. [27] applied MMFE to model deterministic, ensemble, and probabilistic streamflow forecasts and illustrated that ensemble and probabilistic forecasts are more effective than a deterministic forecast. MMFE formulates the total forecast uncertainty of a streamflow in one future period as the sum of forecast improvements in the intermediate periods. This study tests the assumptions of MMFE, i.e., single-period forecast improvements are unbiased, Gaussian distributed, temporally independent, and stationary. Furthermore, this study proposes a generalized martingale model GMMFE to address cases wherein the assumptions are violated.

The remainder of this paper is organized as follows: Section 2 presents a mathematical formulation of the uncertainty evolution of real-time streamflow forecasts and introduces MMFE and its assumptions. Section 3 describes the statistical tests of the assumptions and the results. Section 4 illustrates the GMMFE model used to formulate the evolution of non-Gaussian forecast uncertainties. Section 5 applies the GMMFE in evaluating the effect of forecast uncertainty distributions on reservoir operations. Finally, Section 6 contains the discussions and conclusions.

2. Methods

Streamflow forecasts are updated in real-time. At the beginning of one time period, forecasts of streamflow in the subsequent time periods are made based on currently available hydrologic information. As time progresses and as more hydrologic information becomes available, the forecasts are dynamically updated. This section introduces the MMFE, which describes this dynamic forecast-updating process.

2.1. Mathematical formulation of uncertainty evolution

$f_{s,t}$ is denoted as the forecast made at period s for the streamflow at period t (s must be less than or equal to t). The forecasts made at period s form a vector $F_{s,-}$ comprising $f_{s,s+i}$ ($i = 0,1,\ldots,h$; h denotes the forecast horizon) with lead time ranging from 0 to h periods, i.e.,

$$F_{s,-} = \begin{bmatrix} f_{s,s} & f_{s,s+1} & \cdots & f_{s,s+h} \end{bmatrix} \tag{1}$$

In subsequent periods $s+1, s+2,\ldots, F_{s+1,-}, F_{s+2,-},\ldots$, are made. A schematic of the rolling horizon process of a real-time streamflow forecast with a forecast horizon h (h is set as 4 periods for example) is given at the upper part of Fig. 1.

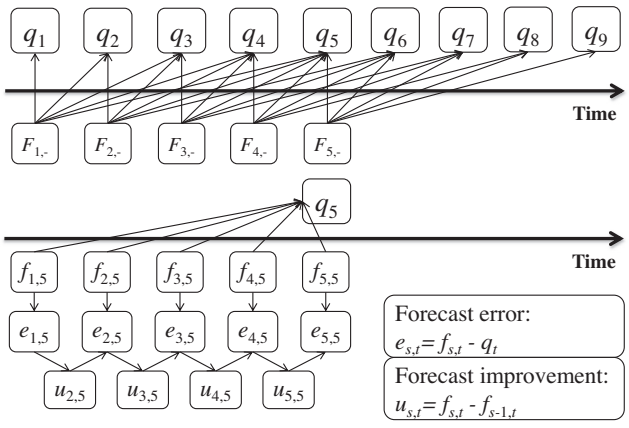

Fig. 1. Schematic of uncertainty evolution in real-time streamflow forecasting.

On one hand, $F_{s,-}$ contains multiple forecasts of streamflow in the subsequent h periods. On the other hand, streamflow q_t at period t corresponds to multiple forecasts made at the precedent periods, as shown in the lower part of Fig. 1. The $h+1$ forecasts $f_{t-i,t}$ ($i = h,\ldots,1,0$) corresponding to q_t form a vector $F_{-,t}$ ($F_{-,t}$ is differentiated from $F_{s,-}$)

$$F_{-,t} = \begin{bmatrix} f_{t-h,t} & f_{t-h+1,t} & \cdots & f_{t,t} \end{bmatrix} \tag{2}$$

The relationship among $f_{s,t}$ (the estimated value), q_t (the real value), and $e_{s,t}$ (the forecast error) are additive [8,24,27]

$$e_{s,t} = f_{s,t} - q_t \tag{3}$$

The forecast errors of $F_{-,t}$ also form a vector $E_{-,t}$

$$E_{-,t} = \begin{bmatrix} e_{t-h,t} & e_{t-h+1,t} & \cdots & e_{t,t} \end{bmatrix} \tag{4}$$

with $e_{s,t}$ ($s = t-h, t-h+1,\ldots,t$), forecast improvement $u_{s,t}$ can be defined as the difference between the forecast errors of two consecutive periods

$$\begin{aligned} u_{s,t} &= e_{s,t} - e_{s-1,t} \\ &= (f_{s,t} - q_t) - (f_{s-1,t} - q_t) \\ &= f_{s,t} - f_{s-1,t} \end{aligned} \tag{5}$$

As shown in Eq. (5) and Fig. 1, $u_{s,t}$ represents the improvement in $f_{s,t}$ (the period s forecast of q_t) from $f_{s-1,t}$ (the previous period's forecast of q_t). We have a total of h updates of $u_{s,t}$ ($s = t-h+1, t-h+2,\ldots,t$) for q_t, which correspond to the $h+1$ elements in $E_{-,t}$ and $F_{-,t}$.

Assuming that the observation (denoted as $f_{t,t}$) at the current period is perfect,

$$f_{t,t} = q_t \tag{6}$$

The relationship between $e_{s,t}$ and $u_{s,t}$ can be formulated as follows:

$$\begin{cases} e_{t,t} = 0 \\ e_{t-1,t} = e_{t,t} - u_{t,t} = -u_{t,t} \\ e_{t-2,t} = e_{t-1,t} - u_{t-1,t} = -u_{t,t} - u_{t-1,t} \\ \cdots \\ e_{t-h+1,t} = e_{t-h+2,t} - u_{t-h+2,t} = -\sum_{i=0}^{h-2} u_{t-i,t} \\ e_{t-h,t} = e_{t-h+1,t} - u_{t-h+1,t} = -\sum_{i=0}^{h-1} u_{t-i,t} \end{cases} \tag{7}$$

By incorporating Eq. (7) into Eq. (3), forecast $f_{s,t}$ can be formulated with q_t and $u_{s,t}$ ($s = t-h+1, t-h+2,\ldots,0$)

$$\begin{cases} f_{t,t} = q_t \\ f_{t-1,t} = q_t - u_{t,t} \\ f_{t-2,t} = q_t - u_{t,t} - u_{t-1,t} \\ \cdots \\ f_{t-h+1,t} = q_t - \sum_{i=0}^{h-2} u_{t-i,t} \\ f_{t-h,t} = q_t - \sum_{i=0}^{h-1} u_{t-i,t} \end{cases} \tag{8}$$

The equation also indicates that

$$\begin{cases} f_{t,t} = f_{t-1,t} + u_{t,t} \\ f_{t-1,t} = f_{t-2,t} + u_{t-1,t} \\ \cdots \\ f_{t-h+1,t} = f_{t-h,t} + u_{t-h+1,t} \end{cases} \tag{9}$$

which implies that $f_{s,t}$ continues to be improved by $u_{s,t}$ as s increases from $t-h$ to t, as shown in Fig. 1.

2.2. Martingale model of forecast evolution (MMFE)

Eqs. (1)–(9) present a decomposition approach for modeling the evolution of forecast uncertainty. The total forecast uncertainty, represented by the forecast error, is formulated by single-period forecast improvements. To characterize $u_{s,t}$ ($t = 1,2,\ldots,T$; $t-h<s\leqslant t$), Heath and Jackson [8] proposed MMFE to describe the sequence $U_{s,-}$ ($s = 1,2,\ldots T$), i.e.,

$$U_{s,-}=[u_{s,s}\quad u_{s,s+1}\quad\ldots\quad u_{s,s+h-1}] \tag{10}$$

In Eq. (10), $U_{s,-}$ comprises h elements, whereas $F_{s,-}$ in Eq. (1) comprises $h+1$ elements because $f_{s,s+h}$ is a new forecast with the largest lead-time but without the corresponding forecast improvement.

MMFE makes the following four assumptions for $U_{s,-}$: (1) the mean values of $u_{s,s+i-1}$ ($i = 1,2,\ldots,h$) are zero (unbiasedness); (2) $u_{s,s+i-1}$ ($i = 1,2,\ldots,h$) are Gaussian distributed (Gaussianity); (3) $u_{s1,s1+i-1}$ ($i = 1,2,\ldots,h$) and $u_{s2,s2+j-1}$ ($j = 1,2,\ldots,h$) ($s1$ and $s2$ indicate two different periods) are independent (temporal independence); and (4) the distributions of $u_{s,s+i-1}$ ($i = 1,2,\ldots,h$) do not change with the value of s (stationarity). With these four assumptions, $u_{s,s+i-1}$ ($s = 1,2,\ldots,T$; $i = 1,2,\ldots,h$) can be described by the variance–covariance matrix of $U_{s,-}$

$$VCV=\begin{bmatrix}\mathrm{var}_1 & \mathrm{cov}_{1,2} & \cdots & \mathrm{cov}_{1,h}\\ \mathrm{cov}_{2,1} & \mathrm{var}_2 & \cdots & \mathrm{cov}_{2,h}\\ \vdots & \vdots & \ddots & \vdots\\ \mathrm{cov}_{h,1} & \mathrm{cov}_{h,2} & \cdots & \mathrm{var}_h\end{bmatrix} \tag{11}$$

where var_i denotes the variance of $u_{s,s+i-1}$, i.e., the magnitude of the uncertainty of a single improvement, and $\mathrm{cov}_{i,j}$ represents the covariance of $u_{s,s+i-1}$ and $u_{s,s+j-1}$. Considering the stationarity assumption, var_i and $\mathrm{cov}_{i,j}$ are identical for all s, i.e., non-time-varying.

Based on the assumptions of unbiasedness and Gaussianity, the uncertainty of $f_{t-i,t}$ can be represented by the variance of the forecast error, i.e., $e_{t-i,t}=f_{t-i,t}-q_t$ (Eq. (3)) and $e_{t-i,t}=-\sum_{j=0}^{i-1}u_{t-j,t}$ (Eq. (7)). Furthermore, based on the assumptions of temporal independence and stationarity, the variance of $e_{t-i,t}$ can be calculated by

$$\mathrm{var}(e_{t-i,t})=\sum_{j=1}^{i}\mathrm{var}_j \tag{12}$$

Eq. (12) indicates that a longer lead-time i results in greater forecast uncertainty. Moreover, the equation also implies that, as time progresses towards t, the uncertainty of $f_{t-i,t}$ decreases.

The MMFE approach was developed and applied to the simulation of demand forecast in supply chain management [8]. Zhao et al. [27] applied MMFE to simulate deterministic, ensemble, and probabilistic streamflow forecasts. Although not a forecast model, MMFE remains a useful statistical model that can simulate the uncertainty evolution of streamflow forecasts. In certain applications, MMFE can generate synthetic forecasts based on streamflow data and the variance–covariance matrix, thus presenting possible forecast scenarios of the future [8,27]. The applications of MMFE basically include two steps. The first step is the specification of the variance–covariance matrix VCV (Eq. (11)), followed by a synthetic generation of $u_{s,s+i-1}$ ($i = 1,2,\ldots,h$) through the Cholesky decomposition of VCV. By assembling $u_{s,s+i-1}$, $U_{-,t}$ can be obtained as

$$U_{-,t}=[u_{t-h+1,t}\quad u_{t-h+2,t}\quad\ldots\quad u_{t,t}] \tag{13}$$

Furthermore, with $U_{-,t}$ and the given q_t ($t = 1,2,\ldots,T$), $E_{-,t}$ (Eqs. (4) and (7)) and $F_{-,t}$ (Eqs. (2) and (8)) can be synthetically generated.

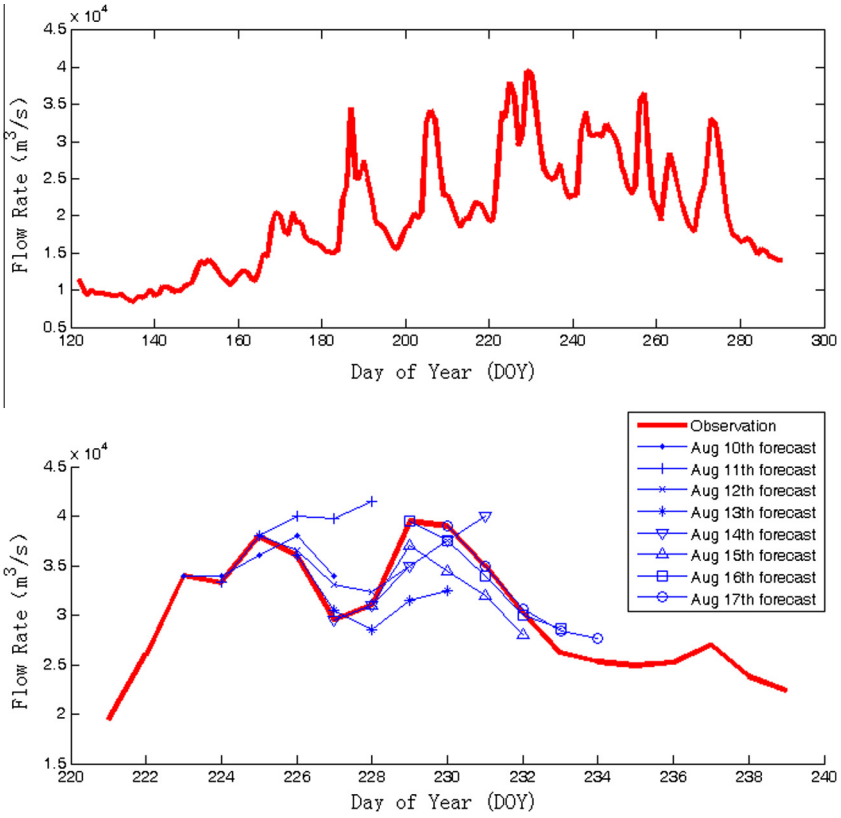

Fig. 2. Daily updated streamflow forecasts of TGR in 2008.

3. Test of model assumptions

MMFE provides an effective decomposition approach for modeling the stochastic process of forecast uncertainty evolution based on the four assumptions. When applying the MMFE model to real-world studies, the validity of the assumptions must be verified. This section applies real-world forecast data on the Three Gorges Reservoir (TGR) to test the assumptions.

3.1. Description of data and statistical tests

TGR controls flooding events in the upper Yangtze River and plays a key role in the flood protection of the middle and the lower reaches of this river [5,12,22]. To aid in the operation of the TGR, inflow forecasts are made based on the main upstream flow, the tributary flow from the Wu River, and the flow from the TGR intervening basin [12]. The intervening basin has a catchment area of 55,907 km^2 (approximately 5.6% of the drainage area of TGR) but contributes to 20% of the flood peaks of TGR inflow on average [12,22]. The complex terrain of the intervening basin makes the prediction of TGR inflow reliably at a long lead time difficult. The current inflow forecast of TGR is updated daily with a forecast horizon of 4 d. This study applies the forecast data of the TGR from May to September in 2004–2009 to test the assumptions of MMFE. Fig. 2 presents an example of the rolling-horizon forecast of the largest flood in 2008. For the flood peak occurring around August 16th (DOY 229), the forecast improved as time progressed toward August 16th, finally ending at zero at the time of observation.

To test the four assumptions of MMFE, the data processing procedure was employed as follows: First, the forecast error sequence $E_{-,t}$ was calculated with the rolling horizon forecast $F_{s,-}$ (Eqs. (3) and (4)). The forecast update $u_{s,t}$ was then calculated based on the forecast error sequence (Eq. (5)). Finally, the forecast updates were arranged as $U_{s,-}$ and $U_{-,t}$ (Eqs. (10) and (13)). $U_{s,-}$ and $U_{-,t}$ in May/June (MJ, the pre-flood season) and July/August/September (JAS, the main flood season) were separated and tested independently. The statistical tests of the assumptions and the dataset are summarized in Table 1.

(1) Test of unbiasedness: The null hypothesis is that the mean value of $u_{s,s+i-1}$ ($i = 1,2,\ldots,4$) in $U_{s,-}$ is zero. The test applies the bootstrap method to draw the N independent random sample sets with replacements from the sample population [7]. The confidence interval of the mean value of $u_{s,s+i-1}$ is estimated based on the mean values of N random sample sets. If the confidence interval contains zero, the null hypothesis is accepted; otherwise, the null hypothesis is rejected.

(2) Test of Gaussianity: The null hypothesis is that the $u_{s,s+i-1}$ ($i = 1,2,\ldots,4$) fits Gaussian distribution. The Shapiro–Wilk test investigates the null hypothesis that the samples came from a normally distributed population. If $u_{s,s+i-1}$ does not fit Gaussian distribution, the test rejects the null hypothesis.

(3) Test of temporal independence: The null hypothesis is that $U_{-,t} = [u_{t-3,t}, u_{t-2,t}, u_{t-1,t}, u_{t,t}]$ (the improvements of forecast of q_t at different periods) are independent. The correlation assesses the linear dependence relationship between two random variables. If no dependence relationship exists, the correlation is zero. As a comparison, this study also tests the cross-correlation among $U_{s,-} = [u_{s,s}, u_{s,s+1}, u_{s,s+2}, u_{s,s+3}]$ (the updates made at the same period). Considering that $u_{s,t}$ can be non-Gaussian, the non-parametric Spearman correlation is used, and the corresponding p-value (i.e., the probability of obtaining a test statistic at least as extreme as the one that was actually observed) indicates statistical significance.

(4) Test of stationarity: The null hypothesis is that $u_{s,s+i-1}$ ($i = 1,2,\ldots,4$) in MJ and $u_{s,s+i-1}$ ($i = 1,2,\ldots,4$) in JAS have the same distribution. The two-sample Kolmogrov–Smirnov test is applied to compare the cumulative distribution functions (CDF) of $u_{s,s+i-1}$ in MJ (the pre-flood season) and JAS (the main flood season). If the two CDFs are different, the test rejects the null hypothesis; otherwise, the null hypothesis is accepted.

Table 1
Statistical tests and datasets applied to testing the assumptions of the MMFE.

Assumptions	Statistical tests	Datasets
Unbiasedness	Bootstrap based test	$U_{s,-}$ in MJ and JAS
Gaussianity	Shapiro–Wilk test	$U_{s,-}$ in MJ and JAS
Temporal independence	Spearman correlation	$U_{-,t}$ and $U_{s,-}$ in JAS
Stationarity	Two-sample Kolmogrov–Smirnov test	$U_{s,-}$ in MJ and JAS

The tests are conducted using the Hypothesis Test Toolbox of Matlab 2010a.

3.2. Test of unbiasedness

Table 3 presents the mean values of the sample and the 95% confidence intervals derived by the bootstrap test. All mean values are positive, which implies that the forecast of TGR is biased and tends to underestimate the actual streamflow. The null hypotheses for $u_{s,s}$ (MJ), $u_{s,s+2}$ (MJ), $u_{s,s+3}$ (MJ), $u_{s,s+2}$ (JAS), and $u_{s,s+3}$ (JAS) are rejected. Although the confidence intervals of $u_{s,s+1}$ (MJ), $u_{s,s}$ (JAS), and $u_{s,s+1}$ (JAS) include the zero value, they are near the lower bound. Based on Table 2, the null hypothesis that the mean value of $u_{s,s+i-1}$ ($i = 1,2,\ldots,4$) is zero is generally rejected. The mean values of $[u_{s,s}, u_{s,s+1}, u_{s,s+2}, u_{s,s+3}]$ are positive, and their confidence intervals also tend to be positive. Therefore, the forecasts of TGR in both the pre- and main flood seasons tend to be underestimations of the actual streamflow.

3.3. Test of Gaussian distribution

In the test for Gaussianity, the Shapiro–Wilk test rejects the null hypothesis when the significance level is set at 1%, which means that the distribution of $u_{s,s+i-1}$ ($i = 1,2,\ldots,4$) is unlikely (the probability is less than 1%) to be Gaussian. To illustrate the non-Gaussian distribution, the quantiles of the samples $[u_{s,s}, u_{s,s+1}, u_{s,s+2}, u_{s,s+3}]$ are plotted against the theoretical quantiles from the Gaussian fits in Fig. 3. If the two distributions being compared are similar, there would have been a linear relationship between the quantiles. However, the quantile–quantile plot shows no linear relationship between the quantiles. Moreover, the positive and negative extreme values of the samples have a wider range than the Gaussians.

Table 2
Sample means and 95% confidence intervals for MJ and JAS.

	The pre-flood season (MJ)		The main flood season (JAS)	
	Sample mean (m^3/s)	95% confidence interval (m^3/s)	Sample mean (m^3/s)	95% confidence interval (m^3/s)
$u_{s,s}$	119.0	[2.7,265.0]	16.5	[−79.1,131.7]
$u_{s,s+1}$	137.1	[−2,317.3]	82.9	[−41.8,243.8]
$u_{s,s+2}$	306.3	[144.2,497.1]	336.4	[162.3,536.6]
$u_{s,s+3}$	368.5	[194.0,591.0]	693.2	[466.0,953.7]

Table 3
p-values of the two-sample Kolmogrov–Smirnov test of the distributions of forecast improvements.

	$u_{s,s}$	$u_{s,s+1}$	$u_{s,s+2}$	$u_{s,s+3}$
MJ vs. JAS	0.078	0.020	0.055	0.051
July vs. August	0.892	0.175	0.219	0.402
August vs. September	0.893	0.829	0.342	0.123
September vs. July	0.924	0.591	0.479	0.362

Fig. 3 confirms the rejection of the null hypothesis of Gaussian distribution in the Shapiro–Wilk test. Furthermore, we find that the approximation of forecast improvements by Gaussian distributions results in the loss of information on extreme values [19].

3.4. Test of temporal independence

$U_{-,t} = [u_{t-3,t}, u_{t-2,t}, u_{t-1,t}, u_{t,t}]$ represents the forecast improvements targeted at the same q_t. The time periods when the forecast improvements were made are different. The scatter plots of $U_{-,t}$ are presented in Fig. 4. The corresponding *p*-values for the cross correlations of $U_{-,t}$ are greater than 5%, which suggests an acceptance of the null hypothesis of temporal independence, i.e., forecast improvements made at different periods are independent. Furthermore, the scatter plots of $U_{s,-} = [u_{s,s}, u_{s,s+1}, u_{s,s+2}, u_{s,s+3}]$ (forecast improvements made at the same period *s*) are presented as a comparison. Fig. 5 shows that $U_{s,-}$ exhibits strong cross correlations, with the *p*-values of the correlations being less than 1%.

The forecast improvements can generally be attributed to the updates of hydrological information, e.g., watershed initial conditions and weather forecasts [10,16,20]. The progression $U_{-,t} = [u_{t-3,t}, u_{t-2,t}, u_{t-1,t}, u_{t,t}]$ results from updates of hydrologic information at different periods, whereas the collection $U_{s,-} = [u_{s,s}, u_{s,s+1}, u_{s,s+2}, u_{s,s+3}]$ can be attributed to the update of hydrologic information at the same period. The independence of $U_{-,t}$ and the dependence of $U_{s,-}$ implies that the update of hydrologic information can exhibit temporal independence relationships. Otherwise, more information could be inferred from the currently available hydrologic information.

3.5. Test of stationarity

The two-sample Kolmogrov–Smirnov test examines the similarity of the CDF of $u_{s,s+i-1}$ ($i = 1,2,\ldots,4$) in MJ and JAS. The test also compares $u_{s,s+i-1}$ ($i = 1,2,\ldots,4$) in July with August, August with September, and September with July. The *p*-values, i.e., the probability of obtaining a test statistic that is at least as extreme as the observed one, of the tests are listed in Table 3. The *p*-values in the case MJ vs. JAS are lower than 0.100, which indicates that the probability that the distributions of $u_{s,s+i-1}$ ($i = 1,2,\ldots,4$) in the pre- and the main flood seasons are the same is less than 10%. Moreover, the *p*-values of the other three cases (July vs. August, August vs. September, and September vs. July) are larger than 0.100, implying that the distributions of $u_{s,s+i-1}$ ($i = 1,2,\ldots,4$) in July, August, and September are likely to be the same. The results shown in Table 3 generally suggest that $u_{s,s+i-1}$ ($i = 1,2,\ldots,4$) is non-stationary in the pre- and main flood seasons, but $u_{s,s+i-1}$ can be stationary during the main flood season.

3.6. Implications from statistical tests

The results of the statistical tests based on streamflow forecast records of TGR illustrate that: (1) real-world forecasts are biased and tend to underestimate the actual streamflow; (2) the forecast improvements do not follow a Gaussian distribution, and their distributions are heavy-tailed; (3) forecast improvements made at different periods are independent, but those made at the same period are dependent; and (4) forecast improvements are not stationary.

The four assumptions of MMFE enable applications of the variance–covariance matrix to simulate the evolution of forecast uncertainty [8,27]. The rejections of unbiasedness and Gaussianity indicate that variance–covariance is insufficient to simulate the evolution of real-world forecast uncertainty and that more information about statistical distribution is needed. The rejection of stationarity indicates that different distributions should be specified for forecast improvements in different seasons. Nevertheless, the acceptance of temporal independence enables the period-by-period independent simulation of $U_{s,-}$ ($s = 1,2,\ldots,T$).

In the following section, we focus on the handling of biased non-Gaussian forecast uncertainty during the main flood season.

4. Accounting for non-Gaussian forecast uncertainties

This section proposes a generalized martingale model called GMMFE to deal with biased, non-Gaussian forecast improvements. The new model incorporates the normal quantile transform (NQT) method into MMFE. This section demonstrates the applications of

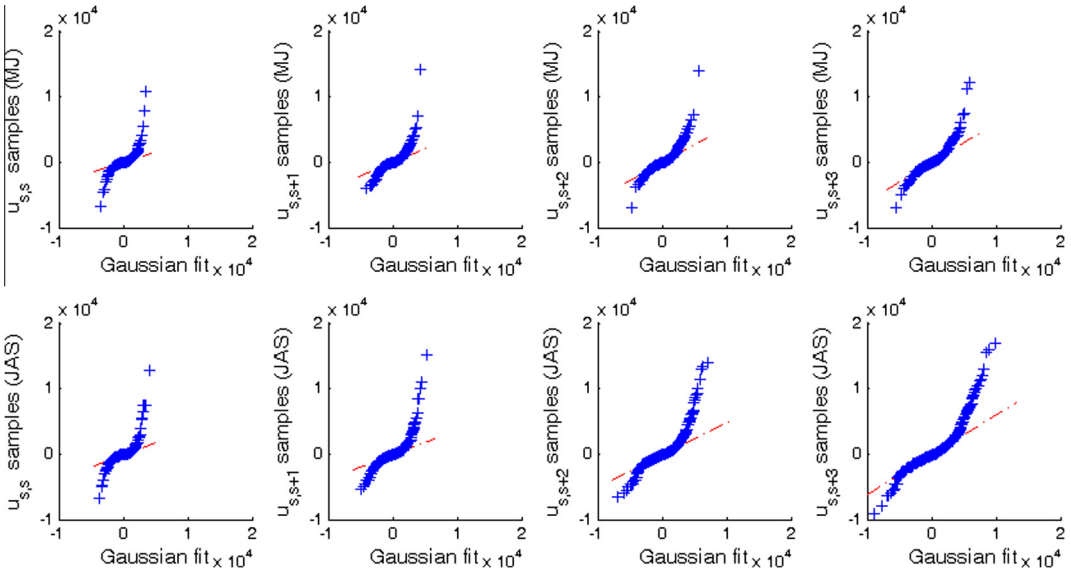

Fig. 3. Quantile–quantile plot of the sample quantiles of forecast improvements against the theoretical quantiles from the Gaussian fits.

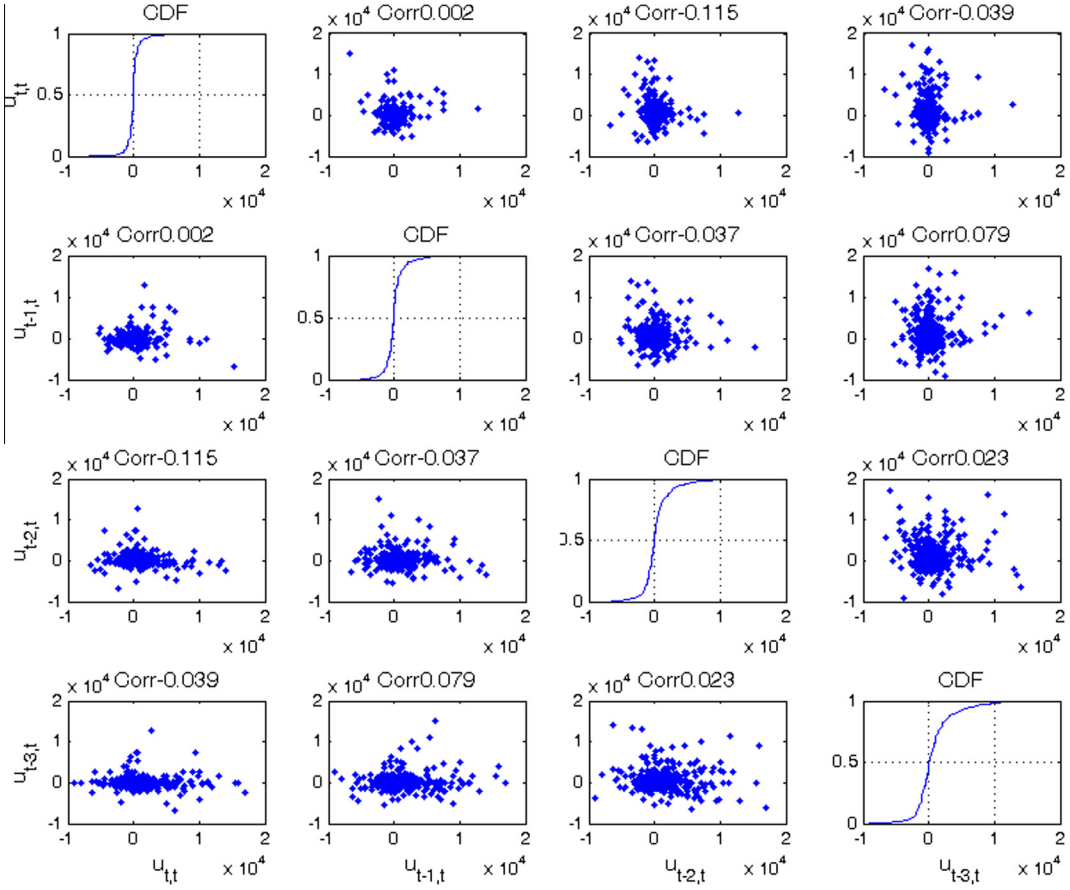

Fig. 4. Scatter plots and Spearman cross correlations of $U_{-,t}$ in the main flood season.

the new model using simulated and observed forecasts from the TGR.

4.1. Generalized martingale model

The MMFE model deals with unbiased Gaussian samples and synthesizes the unbiased Gaussian forecast improvements based on the variance–covariance matrix [8,27]. However, the non-Gaussian properties of forecast improvements hinder the application of MMFE in real-world studies. To bridge this gap, this study integrates the NQT method, which can convert biased non-Gaussian distributed variables into unbiased Gaussian variables [11,15], with the conventional MMFE model. This new model GMMFE comprises three steps: NQT, MMFE, and inverse-NQT, as shown in Fig. 6.

(1) Step 1 is the transformation of variables by NQT. $u_{s,s+i-1}$ $(i = 1,2,\ldots,h)$ are converted into standard Gaussian random variables $u'_{s,s+i-1}$ $(i = 1,2,\ldots,h)$ based on

$$u'_{s,s+i-1} = CDF^{-1}_{Gaussian}(CDF_i(u_{s,s+i-1})) \tag{14}$$

where $CDF_i()$ is the CDF of $u_{s,s+i-1}$, and $CDF^{-1}_{Gaussian}()$ is the inverse of the CDF of standard Gaussian distribution. Eq. (14) comprises two sub-steps. First, $CDF_i()$ transforms $u_{s,s+i-1}$ into the corresponding cumulative probability, which is uniformly distributed between 0 and 1. Thereafter, $CDF^{-1}_{Gaussian}()$ converts the cumulative probabilities into the standard Gaussian random $u'_{s,s+i-1}$. The principle behind NQT is similar to that of the quantile–quantile plot [19] in that the two random variables are matched based on the values of their cumulative probability.

(2) Step 2 is the application of MMFE to the transformed variables. The variance–covariance of $u'_{s,s+i-1}$ $(i = 1,2,\ldots,h)$ is calculated, after which u'_i $(i = 1,2,\ldots,h)$ is generated based on the Cholesky decomposition of the variance–covariance matrix. Both u'_i $(i = 1,2,\ldots,h)$ and $u'_{s,s+i-1}$ $(i = 1,2,\ldots,h)$ are standard Gaussian random variables that have the same cross correlation relationships.

(3) Step 3 is the inverse transformation of the variables by NQT. u'_i $(i = 1,2,\ldots,h)$ and forecast improvements u_i $(i = 1,2,\ldots,h)$ are generated with the inverse application of NQT

$$u_i = CDF^{-1}_i(CDF_{Gaussian}(u'_i)) \tag{15}$$

In Eq. (15), $CDF_{Gaussian}()$ converts u'_i into the corresponding cumulative probability, whereas $CDF^{-1}_i()$ converts the cumulative probabilities into new forecast updates u_i $(i = 1,2,\ldots,h)$. Notably, $CDF^{-1}_i()$ plays an important role in determining the statistical distribution of u_i $(i = 1,2,\ldots,h)$. For example, the substitution of $CDF^{-1}_i()$ with the inverse of the *CDF*s of other distributions, e.g., $N(\mu_i, \sigma_i^2)$, enables u_i to fit the Gaussian distribution with mean μ_i and standard deviation σ_i.

When applying GMMFE to real-world cases, these three steps are needed, and special attention should be focused on fitting the CDF for the given samples of $u_{s,s+i-1}$ $(i = 1,2,\ldots,h)$. However, the first step of NQT for handling given samples is unnecessary for hypothetical studies. On the other hand, the two steps of MMFE and inverse-NQT are needed. The variance–covariance matrix should be set for Step 2 to account for the dependence relationships [8,9]. $CDF^{-1}_i()$ $(i = 1,2,\ldots,h)$ should be specified for Step 3 to determine the statistical distribution of forecast improvements.

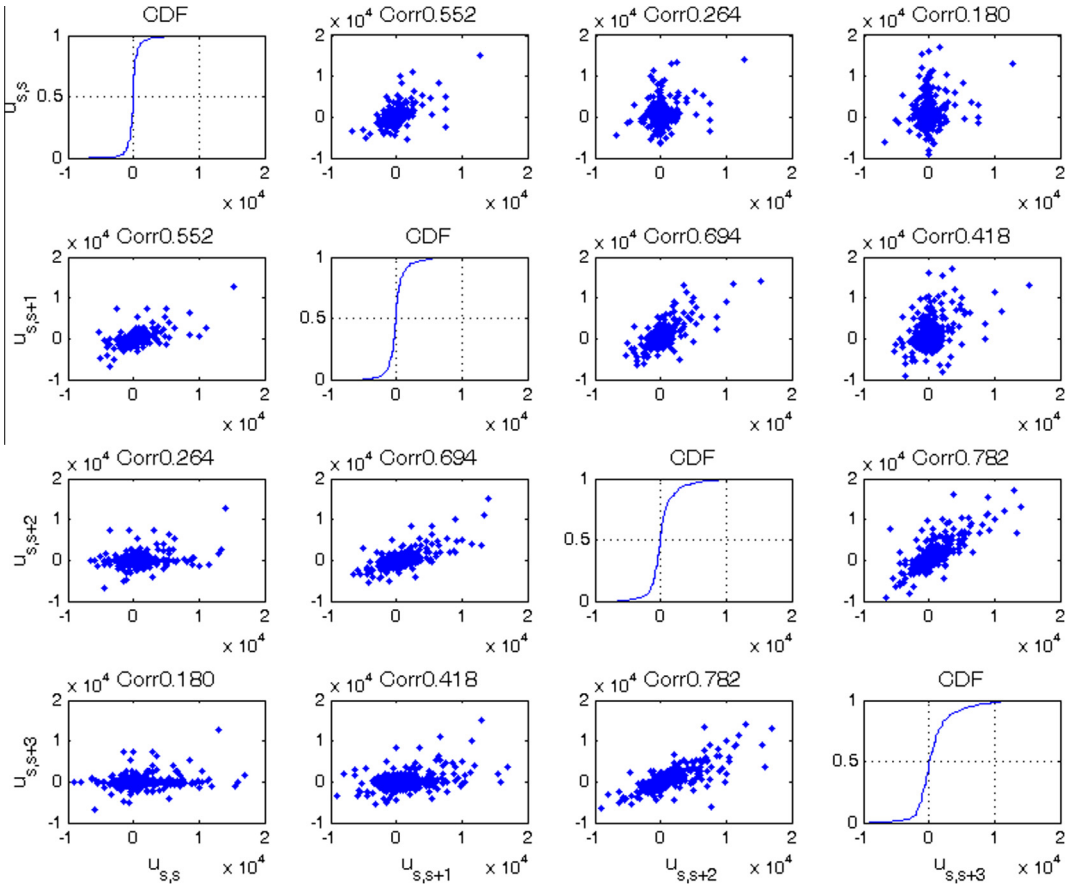

Fig. 5. Scatter plots and Spearman cross correlations of $U_{s,-}$ in the main flood season.

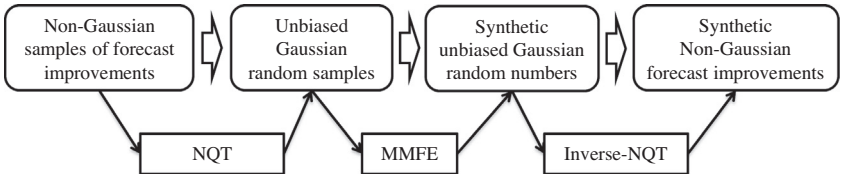

Fig. 6. Flowchart of the generalized martingale model of forecast evolution (GMMFE).

In a simple case where forecast improvements in each period (Eq. (10)) are assumed to be independent, only Step 3 is needed, and u_i ($i = 1,2,\ldots,h$) can be individually simulated. The streamflow forecast can then be synthesized based on Eqs. (1)–(9).

4.2. Simulation of streamflow forecast

The GMMFE model is applied to generate synthetic streamflow forecast improvements for the TGR during the main flood season of 2008 (Fig. 2). The CDF of $u_{s,s+i-1}$ ($i = 1,2,\ldots,h$) samples are estimated by the non-parametric kernel density function [17]. To examine the effects of the assumptions of unbiasedness and Gaussianity, three cases are designed:

(1) In the case UG, $CDF_i^{-1}()$ in Eq. (15) is substituted by the inverse of the *CDF* of $N(0,\sigma_i^2)$, and u_i fits unbiased Gaussian distribution;
(2) In the case BG, $CDF_i^{-1}()$ is substituted by the inverse of the *CDF* of $N(\mu_i,\sigma_i^2)$, and u_i fits the biased Gaussian distribution; and
(3) In the case NG, $CDF_i^{-1}()$ is represented by the inverse of the kernel cumulative density function, and u_i fits the non-Gaussian distribution. In the cases of UG and BG, μ_i and σ_i denote the mean and the standard deviation of the $u_{s,s+i-1}$ ($i = 1,2,\ldots,h$; $h = 4$) samples of the main flood season in 2008, respectively.

The GMMFE model generates forecast improvements at each period (Eq. (10)) and simulates streamflow forecast (Eqs. (7) and (8)). We run 100 Monte-Carlo simulations with GMMFE and derive the forecast errors of synthetic forecast with a lead-time of 1 d to 4 d for the three cases. The mean, standard deviation (stdev), and the coefficient of skewness (C_s) of the forecast errors are presented by boxplots, as shown in Fig. 7. The boxplots illustrate the median as a central mark, the 25th and 75th percentiles as edges, the range of data points as whiskers, and the outliers as plus signs. For comparison, the statistics of the forecast errors of the TGR streamflow forecast records are represented by the circles linked by a line in Fig. 7.

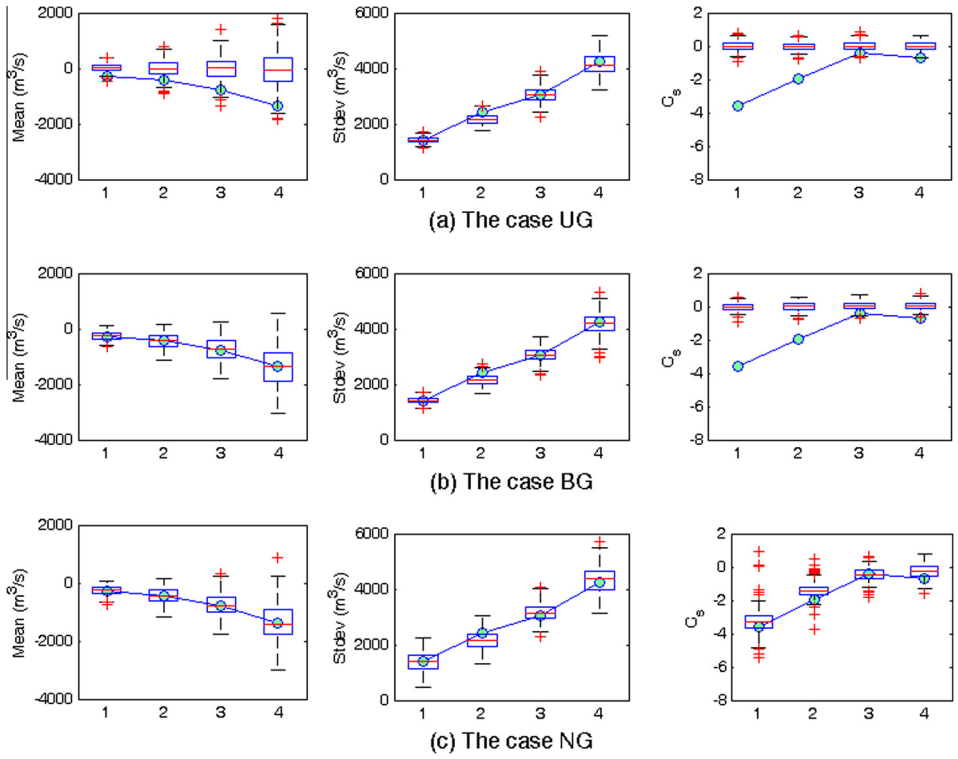

Fig. 7. Distribution of the means, standard deviations, and coefficients of skewness of the observed and simulated forecast errors (circles linked by a line represent observed statistics, whereas boxplots are for simulated statistics).

The effect of the violation of the unbiasedness assumption is detected by the mean value in the case UG, which shows that this assumption results in the underestimation of the forecast error by approximately 1000 m^3/s when the lead time is 4 d. The effect of the violation of the Gaussianity assumption is illustrated by the C_s values in the cases of UG and BG, which indicates that this assumption results in the underestimation of the skewness of the forecast errors because Gaussian distribution is symmetric. The case of NG considers both unbiased and non-Gaussian forecast uncertainty, which results in statistics of synthetic forecast errors similar to actual values. In summary, the three cases demonstrate the effectiveness and generality of the GMMFE model in simulating evolution of forecast uncertainties.

5. Effect of forecast uncertainty distribution on reservoir operation

This study examines the non-Gaussian forecast uncertainties for the TGR. Notably, real-world forecast uncertainties are complex and are dependent on forecast models and hydrological characteristics. Thus, such uncertainties can be Gaussian, biased Gaussian, or non-Gaussian. Simply assuming a Gaussian distribution for the streamflow forecast may set incorrect expectations on the operation results in some cases. The GMMFE model is capable of simulating forecast uncertainties with different statistical distributions. Therefore, this section evaluates the effects of unbiased Gaussian, biased Gaussian, and non-Gaussian forecast uncertainties on reservoir operation using streamflow forecasts generated by GMMFE.

5.1. Rolling-horizon reservoir operation

Reservoir operation utilizes a rolling-horizon process to incorporate the dynamically updated streamflow forecast into decision-making [3,18,28]. This study employs a hypothetical reservoir and synthesizes streamflow forecasts for reservoir operation. The reservoir operation model aims to maximize total utility, i.e.,

$$\max \quad \sum_{i=1}^{n} g_i(r_i)$$
$$s.t. \quad \begin{cases} s_i + x_i - r_i = s_{i+1} \quad (i = 1, \ldots, n) \\ s_{\min} \leqslant s_i \leqslant s_{\max} \quad (i = 1, \ldots, n) \\ s_1 = s_{ini} \\ s_{n+1} = s_{end} \\ r_i \geqslant r_{\min} \end{cases} \tag{16}$$

where i is the index of time periods ranging from 1 (the current period) to n (the operation horizon); s_i denotes the reservoir storage at the beginning of period i; x_i and r_i represent the period i's streamflow forecast and release decision respectively; $s_{\min}$ and $s_{\max}$ are the minimum and the maximum of reservoir storage, respectively; s_{ini} and s_{end} denote initial and ending storage, respectively; and $r_{\min}$ is the lower bound of reservoir release.

In the reservoir operation with a study horizon of T periods, the rolling-horizon process comprises the following steps:

(1) Release decisions are made based on the forecasts made at the current period s

$$[x_1 \quad x_2 \quad \ldots \quad x_n] = [f_{s,s} \quad f_{s,s+1} \quad \ldots \quad f_{s,T}] \tag{17}$$

(2) The current release decision r_1 is implemented, and r_1 is saved as r_s.

(3) The next period $s+1$ is considered, and the initial storage and streamflow forecast are updated:

$$s_{ini} = s_1 + q_s - r_s \tag{18}$$

$$[x_1 \quad x_2 \quad \ldots \quad x_n] = [f_{s+1,s+1} \quad f_{s+1,s+2} \quad \ldots \quad f_{s+1,T}] \tag{19}$$

These three steps are repeated until the end of the study horizon T. The operation horizon n in Eq. (16) notably reduces from T to 1 as s progresses from 1 to T. In each period, the current release decision is saved, and the single-period utility is evaluated. The total utility is the sum of all single-period utilities. Finally, the total utility of the rolling-horizon reservoir operation can be compared with that of the baseline scenario, which is defined as a case without any reservoir regulation. The utility improvement indicates the value of forecast-based reservoir operation.

5.2. Experiment setting

The experiment is set up based on the reservoir operation model given by Zhao et al. [27]. The reservoir takes a concave utility function, i.e., r_i exhibits a diminishing marginal utility (for instance, the case of water supply operation)

$$g_i(r_i) = \begin{cases} \sqrt{\frac{r_i - r_{\min}}{r_{\max} - r_{\min}}} & (r_{\max} \geqslant r_i \geqslant r_{\min}) \\ 1 & (r_i > r_{\max}) \end{cases} \tag{20}$$

The parameters of the reservoir are as follows: $s_{\min} = 0$, $r_{\min} = 0.2$, $r_{\max} = 1.2$, and $s_{ini} = s_{end} = \frac{s_{\max}}{2}$. The study horizon T is set as six periods. Two scenarios are set for $s_{\max}$, i.e., 0.5 and 2.0, examining the effects of reservoir storage capacity [21,28].

The reservoir inflow is generated using a simplified Thomas–Fiering model, i.e.,

$$q_{t+1} = \mu + \rho_{flow}(q_t - \mu) + \sqrt{1 - \rho_{flow}^2}(\mu C_v)\delta \tag{21}$$

where q_t denotes streamflow in period t; δ is a standard Gaussian random number for Monte-Carlo simulation; and the parameters are set as $\mu = 1$, $\rho_{flow} = 0.4$, and $C_v = 0.3$.

The streamflow forecast is generated by GMMFE. To simplify the formulation, $u_{s,t}$ $(t = s, \ldots, T)$ are treated as independent and identically distributed random variables, and $u_{s,t}$ is simulated individually. The skewedness in forecast errors (Fig. 7) is considered by setting the positively and negatively skewed distributions for non-Gaussian forecast uncertainty.

Four cases are designed:

(1) In the case of UG, $u_{s,t}$ is from an unbiased Gaussian distribution with a mean of 0 and a stdev of σ

$$u_{s,t} = \sigma\delta, \delta \sim N(0, 1^2) \tag{22}$$

(2) In the case of BG, $u_{s,t}$ is from a biased and Gaussian distribution with a mean of Δ and a stdev of σ

$$u_{s,t} = \Delta + \sigma\delta, \delta \sim N(0, 1^2) \tag{23}$$

(3) In the case of NGn, $u_{s,t}$ is from a negatively-skewed log-normal distribution with a mean of Δ and a stdev of σ

$$u_{s,t} = \Delta + \sigma(2 - \delta), \delta \sim Logn(2, 1^2) \tag{24}$$

(4) In the case of NGp, $u_{s,t}$ is from a positively-skewed log-normal distribution with a mean of Δ and a stdev of σ

$$u_{s,t} = \Delta + \sigma(\delta - 2), \delta \sim Logn(2, 1^2) \tag{25}$$

In Eqs. (24) and (25), δ is from the log-normal distribution with a mean of 2 and a stdev of 1.

By fixing Δ as 0.05 and varying σ from 0.02 to 0.20, this study generates streamflow forecasts for the four defined uncertainty distributions using GMMFE. The forecasts are incorporated into the rolling horizon reservoir operation. The reservoir optimization model (Eq. 16) is solved by improved dynamic programming (IDP, [29]), which takes advantage of concavity of objective function and improves computational efficiency of conventional dynamic programming. The effects of forecast uncertainty distribution on reservoir operation among the four cases are analyzed by comparing the utility improvements from the baseline case without any reservoir regulation.

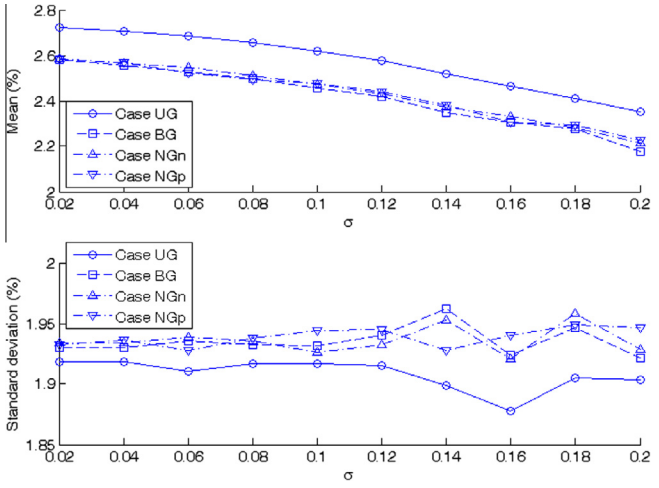

Fig. 8. Relationship of forecast uncertainty with the mean and standard deviation of utility improvements ($s_{\max} = 0.50$).

5.3. Result analysis

This study conducts 100 Monte–Carlo experiments for each σ value and evaluates the utility improvements for the four cases of forecast uncertainty. Fig. 8 presents the utility improvements when reservoir capacity $s_{\max}$ is 0.50. The applications of streamflow facilitate utility improvements in comparison with the baseline case. The mean of the utility improvements decreases, and the stdev of utility improvements tends to slightly increase with increasing σ. Comparing the UG case with the three other cases, the presence of Δ in the BG, NGn, and NGp cases reduces the mean utility improvements and contributes to the increase in standard deviation.

Fig. 9 further presents the utility improvements when reservoir capacity $s_{\max} = 2.0$. Compared with Fig. 8, the applications of streamflow forecast bring about greater but also more variable utility improvements. In the BG, NGn and NGp cases, there are marginal differences in terms of the mean of utility improvements. Moreover, there are minimal differences in the stdev of the utility improvements when σ is small, but major differences in stdev are observed as σ increases. The stdev of the utility improvements exhibits the most rapid increase in the NGp case (biased and positively-skewed forecast uncertainty distribution), followed by BG (biased and Gaussian distribution), NGn (biased and negatively-skewed distribution), and UG (unbiased and Gaussian distribution) cases. A larger reservoir can regulate streamflow at a longer timeframe and exploit forecasts with a longer lead time [21]. However, a streamflow forecast with a longer lead time involves greater uncertainty (Eq. (12)). The effects of the non-Gaussian forecast uncertainty on the reservoir operation are greater in Fig. 9 than in Fig. 8. This finding implies that more attention should be focused on the non-Gaussian characteristics of forecast uncertainty in the operation of larger reservoirs. Given that unbiased-Gaussian distributions are often simply assumed for forecast uncertainties in real cases, Figs. 8 and 9 suggest that this assumption results in the overestimation of the utilities from the applications of the streamflow forecast if the actual uncertainties are not unbiased-Gaussian distributed. Therefore, more attention should be paid to evaluating

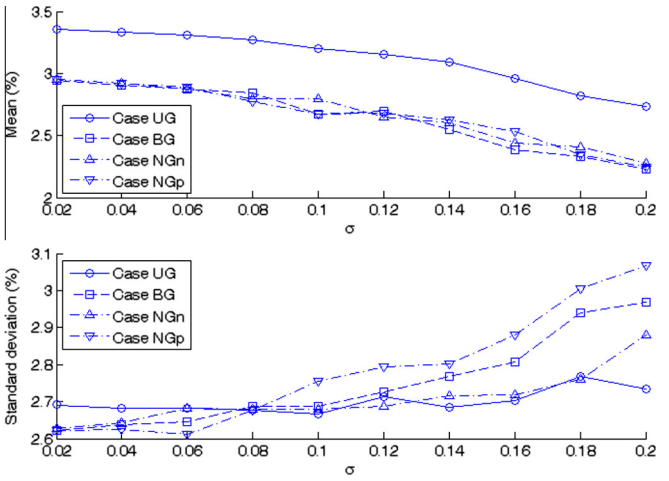

Fig. 9. Relationship of forecast uncertainty with the mean and standard deviation of utility improvements (s_{max} = 2.00).

the statistical distribution of forecast uncertainty before using streamflow forecasts.

Furthermore, the benefit from streamflow forecasts in reservoir operations may vary considerably because of the dependence on a number of factors, e.g., hydrological characteristics, objective functions, and physical constraints [14,21,27]. Thus, the effect of forecast uncertainty distribution on reservoir operations may also vary on a case-by-case basis. However, properly estimating the forecast uncertainty distribution is evidently necessary before utilization, and the GMMFE model provides a general tool to address this issue.

6. Discussions and conclusions

Streamflow forecasts are dynamically updated in real-time, resulting in a process of forecast evolution. The martingale model of forecast evolution (MMFE) provides a conceptual statistical approach for modeling this process. The applicability of MMFE to real-world data depends on four assumptions, i.e., unbiasedness, Gaussianity, temporal independence, and stationarity. This study conducts statistical tests on these four assumptions using streamflow forecast data on the Three Gorges Reservoir (TGR) from 2004 to 2009. The results illustrate that (1) streamflow forecasts are negatively biased; (2) forecast uncertainties are non-Gaussian and heavy-tailed; (3) forecast improvements made at different periods exhibit temporal independence, whereas those made at the same period are dependent; and (4) forecast improvements are non-stationary, and their distributions can vary based on the different seasons of the year.

To address the challenges raised by the statistical tests, this study proposes a new model GMMFE to deal with biased non-Gaussian forecast uncertainties by combining the normal quantile transform (NQT) method with the MMFE model. The GMMFE model comprises three steps. First, the samples of forecast improvement are converted into Gaussian random numbers by NQT to obtain the variance–covariance matrix (*VCV*). Second, new Gaussian random numbers are generated by MMFE with the *VCV*. Finally, new samples of forecast improvements are generated through the inverse application of NQT. We present a study that synthesizes the streamflow forecasts with the GMMFE model, which illustrates the effectiveness and generalizability of the GMMFE.

Based on the characteristics of generality, the GMMFE model is capable of simulating forecast uncertainties with different statistical distributions. Therefore, this paper evaluates the effect of unbiased Gaussian, biased Gaussian, and non-Gaussian forecast uncertainties on reservoir operations, which shows that incorrect assumptions on uncertainty distribution can results in the overestimation of reservoir operation utility. Thus, special attention should be paid to the characteristics of uncertainty distribution when employing forecasts in real-time operations. The proposed GMMFE model provides an effective and generalized tool for addressing this issue.

Acknowledgements

We are grateful to the Editor and the three anonymous reviewers for their constructive suggestions, which have facilitated major improvements in this paper. The authors are also grateful to Grey Nearing for his editorial assistance and to Professor Pan Liu for providing the TGR forecast data. This research was partially supported by the National Natural Science Foundation of China (Project Nos. 51179085 and 50939004) and the Ministry of Science and Technology of China (Project No. 2011BAC09B07).

References

[1] Ajami NK, Duan QY, Sorooshian S. An integrated hydrologic Bayesian multimodel combination framework: confronting input, parameter, and model structural uncertainty in hydrologic prediction. Water Resour Res 2007;43(1). http://dx.doi.org/10.1029/2005WR004745.

[2] Ajami NK, Hornberger GM, Sunding DL. Sustainable water resource management under hydrological uncertainty. Water Resour Res 2008;44(11). http://dx.doi.org/10.1029/2007WR006736.

[3] Alemu ET, Palmer RN, Polebitski A, Meaker B. Decision support system for optimizing reservoir operations using ensemble streamflow predictions. J Water Res PL-ASCE 2011;137(1):72–82. http://dx.doi.org/10.1061/(ASCE)WR.1943-5452.0000088.

[4] Boucher MA, Tremblay D, Delorme L, Perreault L, Anctil F. Hydro-economic assessment of hydrological forecasting systems. J Hydrol 2012;416:133–44. http://dx.doi.org/10.1016/j.jhydrol.2011.11.042.

[5] Cao GJ, Cai ZG, Liu ZW, Wang GQ. Daily optimized model for long-term operation of the Three Gorges–Gezhouba cascade power stations. Sci China Ser E 2007;50:98–110. http://dx.doi.org/10.1007/s11431-007-6010-x.

[6] Carpenter TM, Georgakakos KP. Assessment of Folsom lake response to historical and potential future climate scenarios: 1 Forecasting. J Hydrol 2001;249(1–4):148–75. http://dx.doi.org/10.1016/S0022-1694(01)00417-6.

[7] Efron B. 1977 Rietz lecture – bootstrap methods – another look at the Jackknife. Ann Stat 1979;7(1):1–26. http://dx.doi.org/10.1214/aos/1176344552.

[8] Heath DC, Jackson PL. Modeling the evolution of demand forecasts with application to safety stock analysis in production distribution-systems. IIE Trans 1994;26(3):17–30. http://dx.doi.org/10.1080/07408179408966604.

[9] Ilich N, Despotovic J. A simple method for effective multi-site generation of stochastic hydrologic time series. Stoch Environ Res Risk Assess 2007. http://dx.doi.org/10.1007/s00477-007-0113-6.

[10] Koster RD, Mahanama SPP, Livneh B, Lettenmaier DP, Reichle RH. Skill in streamflow forecasts derived from large-scale estimates of soil moisture and snow. Nature Geosci 2010;3(9):613–6. http://dx.doi.org/10.1038/ngeo944.

[11] Krzysztofowicz R. Transformation and normalization of variates with specified distributions. J Hydrol 1997;197(1–4):286–92. http://dx.doi.org/10.1016/S0022-1694(96)03276-3.

[12] Li XA, Guo SL, Liu P, Chen GY. Dynamic control of flood limited water level for reservoir operation by considering inflow uncertainty. J Hydrol 2010;391(1–2):126–34. http://dx.doi.org/10.1016/j.jhydrol.2010.07.011.

[13] Maurer EP, Lettenmaier DP. Predictability of seasonal runoff in the Mississippi river basin. J Geophys Res ATMOS 2003;108(D16). http://dx.doi.org/10.1029/2002JD002555.

[14] Maurer EP, Lettenmaier DP. Potential effects of long-lead hydrologic predictability on Missouri river main-stem reservoirs. J Clim 2004;17(1):174–86. http://dx.doi.org/10.1175/1520-0442(2004)017<0174:PEOLHP>2.0.CO;2.

[15] Montanari A. Deseasonalisation of hydrological time series through the normal quantile transform. J Hydrol 2005;313(3–4):274–82. http://dx.doi.org/10.1016/j.jhydrol.2005.03.008.

[16] Sankarasubramanian A, Lall U, Devineni N, Espinueva S. The role of monthly updated climate forecasts in improving intraseasonal water allocation. J Appl Meteorol Climatol 2009;48(7):1464–82. http://dx.doi.org/10.1175/2009JAMC2122.1.

[17] Sharma A, Tarboton DG, Lall U. Streamflow simulation: a nonparametric approach. Water Resour Res 1997;33(2):291–308. http://dx.doi.org/10.1029/96WR02839.

[18] Simonovic SP, Burn DH. An improved methodology for short-term operation of a single multipurpose reservoir. Water Resour Res 1989;25(1):1–8. http://dx.doi.org/10.1029/WR025i001p00001.
[19] Tan WD, Gan FF, Chang TC. Using normal quantile plot to select an appropriate transformation to achieve normality. Comput Stat Data Anal 2004;45(3):609–19. http://dx.doi.org/10.1016/S0167-9473(03)00009-4.
[20] Valeriano OCS, Koike T, Yang K, Graf T, Li X, Wang L, Han XJ. Decision support for dam release during floods using a distributed biosphere hydrological model driven by quantitative precipitation forecasts. Water Resour Res 2010;46. http://dx.doi.org/10.1029/2010WR009502.
[21] Vogel RM, Stedinger JR. Generalized storage reliability yield relationships. J Hydrol 1987;89(3–4):303–27. http://dx.doi.org/10.1016/0022-1694(87)90184-3.
[22] Wang BW, Tian FQ, Hu HP. Analysis of the effect of regional lateral inflow on the flood peak of the Three Gorges Reservoir. Sci China Ser E 2011;54(4):914–23. http://dx.doi.org/10.1007/s11431-011-4330-3.
[23] Wei WW, Watkins DW. Data mining methods for hydroclimatic forecasting. Adv Water Resour 2011;34(11):1390–400. http://dx.doi.org/10.1007/s11431-011-4330-3.
[24] Weigel AP, Liniger MA, Appenzeller C. Can multi-model combination really enhance the prediction skill of probabilistic ensemble forecasts? Q J R Meteorol Soc 2008;134(630):241–60. http://dx.doi.org/10.1002/qj.210.
[25] Wood EF et al. Hyperresolution global land surface modeling: meeting a grand challenge for monitoring Earth's terrestrial water. Water Resour Res 2011;47. http://dx.doi.org/10.1029/2010WR010090.
[26] Yao H, Georgakakos A. Assessment of Folsom Lake response to historical and potential future climate scenarios 2. Reservoir management. J Hydrol 2001;249(1–4):176–96. http://dx.doi.org/10.1016/S0022-1694(01)00418-8.
[27] Zhao TTG, Cai XM, Yang DW. Effect of streamflow forecast uncertainty on real-time reservoir operation. Adv Water Resour 2011;34(4):495–504. http://dx.doi.org/10.1016/j.advwatres.2011.01.004.
[28] Zhao TTG, Yang DW, Cai XM, Zhao JS, Wang H. Identifying effective forecast horizon for real-time reservoir operation under a limited inflow forecast. Water Resour Res 2012;48. http://dx.doi.org/10.1029/2011WR010623.
[29] Zhao TTG, Cai XM, Lei XH, Wang H. Improved dynamic programming for reservoir operation optimization with a concave objective function. J Water Resour Plann Manage 2012;138(6):590–6. http://dx.doi.org/10.1061/(ASCE)WR.1943-5452.0000205.